scientific reports

Check for updates

OPEN

On unsteady 3D bio-convection flow of viscoelastic nanofluid with radiative heat transfer inside a solar collector plate

Umar Farooq[1], Hassan Waqas[1], Zahir Shah[2]✉, Poom Kumam[3,4]✉ & Wejdan Deebani[5]

Nanoparticles are used in industrial and engineering by allowing for faster heat transfer rates in microchips, vehicle cooling, food processing, and nuclear reactors. This research aims to scrutinize the three-dimensional bioconvectional flow performances of viscoelastic nanofluids through a elongating sheet with motile microorganisms. Radiative impact and solutal boundary conditions are studied here. The impacts of thermophoresis, Brownian motion, and bioconvection are also considered. By using suitable similarity transformations, the PDEs are converted into ODEs. The numerical and graphical results are calculated with the help of shooting scheme built-in function Bvp4c in computational tool MATLAB. The graphical and numerical importance of physical engineering parameters like local skin friction, local Nusselt, local Sherwood, and local motile microorganism numbers are discussed here. The thermal profile is enhanced for the higher estimations of the Brownian motion and thermophoresis parameter. The heat profile is boosted up for the increasing variations of the thermal radiation and the thermophoresis parameter. The energy profile is improved by increasing the estimations of solutal Biot number while declining for mixed convection parameter and unsteadiness parameter. The microorganism profile decays for Peclet and bioconvection Lewis number while rising for buoyancy ratio parameter and bioconvection Rayleigh number.

List of symbols

u, v, w	Components of velocity (m s^{-1})
δ_1	Microorganisms difference number
α_m	Thermal diffusivity (m^2 s^{-1})
x, y, z	Space coordinates (m)
$(\rho c)_p$	Heat capacity of nanoparticles (J kg^{-3} K^{-1})
γ_1	Thermal Biot number
Lb	Bio convection Lewis number
α	Ratio parameter
β	Viscoelastic fluid parameter
S_1	Thermally stratified parameter
ν	Kinematic viscosity (m^2 s^{-1})
Nn	Microorganism density number
$(\rho c)_f$	Heat capacity of base fluid (J kg^{-3} K^{-1})
S_2	Solutal stratified parameter
S_3	Microorganisms stratified parameter
D_m	Microorganisms diffusivity (m^2 s^{-1})
Pr	Prandtl parameter

[1]Department of Mathematics, Government College University Faisalabad, Faisalabad 38000, Pakistan. [2]Department of Mathematical Sciences, University of Lakki Marwat, Lakki Marwat 28420, Khyber Pakhtunkhwa, Pakistan. [3]Fixed Point Research Laboratory, Fixed Point Theory and Applications Research Group, Center of Excellence in Theoretical and Computational Science (TaCS-CoE), Faculty of Science, King Mongkut's University of Technology Thonburi (KMUTT), 126 Pracha Uthit Rd., Bang Mod, Thung Khru, Bangkok 10140, Thailand. [4]Department of Medical Research, China Medical University Hospital, China Medical University, Taichung 40402, Taiwan. [5]Department of Mathematics, College of Science and Arts, King Abdulaziz University, P.O. Box 344, Rabigh 21911, Saudi Arabia. ✉email: zahir@ulm.edu.pk; poom.kum@kmutt.ac.th

λ	Mixed convective number
b	Chemotaxis constant (m)
ρ_f	Fluid's density (kg m^{-3})
Nr	Buoyancy-ratio parameter
γ_2	Solutal Biot number
Nb	Brownian motion number
Nc	Bio convection Rayleigh number
W_c	Speed of cell swimming (m s^{-1})
Nt	Thermophoresis number
Le	Lewis number
γ_3	Microorganisms stratification Biot number
Pe	Peclet parameter
Nu	Nusselt number
Sn	Sherwood number
D_B	Brownian diffusivity (m^2 s^{-1})
D_T	Thermophoresis diffusivity (m^2 s^{-1})
N	Microorganisms
$a_1^*, a_2^*, a_3^*, d_1^*, d_2^*, d_3^*$	Dimensionless constants

Because of their many uses in engineering and science, nanofluids pique the interest of many researchers. Nanostructures are well-known as heat transfer coolants and are often used to avoid mobile system overheating. Furthermore, nanofluid cleaning products, micro-cryosurgery, automotive evolve from biological and environmental, and computer chips use nanofluids. Choi[1] proposed the central principle of nanoliquid in 1995, which has since been expanded upon by many researchers. Buongiorno[2] studied nanomaterials convection transfer by taking Brownian and thermophoresis diffusion properties into account. Hsiao[3] numerically investigated micropolar nanofluid flow with multifaceted properties such as viscous diffusion and magnetic field. Turkyilmazoglu[4] investigated the significance of nanomaterials in an asymmetrical channel using the well-known Buongiorno model. Alblawi et al.[5] used the Buongiorno model of curve extended geometry to investigate nanoparticles in thermo physics. Khan and Pop[6] investigated the movement of nanofluids through the Buongiorno model after it had gone via the stretched surface. Multiwall carbon nanotubes in nanofluid boundary layer flow were investigated by Shafiq et al.[7]. Hayat et al.[8] investigated the diffusion implications on the transportation of viscoelastic nanofluids via extensible walls. The flow of nanoliquid in porous media was studied by Hayat et al.[9]. By changing the structure, Azam et al.[10] studied the characteristics of Carreau nanoliquid flow. Elgazery[11] deals with the theoretical connection of four different types of nanoparticles characteristics. Ahmad et al.[12] investigated three-dimensional nanofluid flow with Brownian motion and thermophoresis. The flow of the Buongiorno model through a conductive and considerably expanded network was reported by Alblawi et al.[5]. Hayat et al.[13] used nanomaterials power to study the flow of MHD nanofluids across a non-linear surface. Asma et al.[14] looked at 3D nanofluid magnetized flow caused by energy activation and heat generation/absorption caused by a spinning disc issue. Eid et al.[15] studied the Carreau nanofluid flow above a nonlinear moving surface using chemical and heat absorption/generation techniques. Al-Bashir et al.[16] investigated cell heat and solar radiation. Sohail et al.[17] studied the fluid in the presence of thermal radiations. Nader et al.[18] investigated a photovoltaic system with a refrigeration system. Hussien et al.[19] conducted a brief study into the heat transfer of nanofluids. Abu-Libdeh et al.[20] investigated the entropy of a hybrid nanofluid on a highly permeable cavity. Hussien et al.[21] explored the heat transfer of hybrid nanofluids in the presence of thermal radiation. Al-Kouz et al.[22] investigated the role of heat transfer with nanocomposites in chemical reactions. Mahesh et al.[23] looked into the importance of hybrid Nanofluid flow over discs with entropy generation enhancement. Mahanthesh et al.[24] investigated the aspects of quadratic convection on dusty nanofluid on a vertical surface. Owhai et al.[25] investigated the effects of a given prescription heat flux on nanoliquid. Attempts[26–33] indicate investigators' additional research in the field of nanofluids. Over the last decade, through use of nanofluids in solar collectors has gotten a lot of scientific interest. Nevertheless, there are significant gaps in the research on the use of oil-based nanoliquid in solar panels, as there isn't enough material, particularly practical studies, available. This work aims to add to the existing body of knowledge by demonstrating the results of the two new oil-based hybrid nanofluids in a solar collector. The thermal efficiency and heat transmission capabilities of the nanofluids were assessed. The research provides a green approach to the synthesis of nanomaterials for application in solar collectors. OLE-ZVI and OLE-TiO_2 are two nanoparticles made from the almond extract of leaves. The impacts of nanofluids on exert economic efficiency, thermal expansion, and hydraulic gradient anywhere along PTC's suction pipe are included in a performance assessment of the collector. In addition, we offer a comparison of our findings to those available in the literature. A reflector sheet curved in a parabola form and a receiver's tube positioned at a focal length from either the reflected sheet make up the collectors. The reflecting sheet (mirror) collects direct solar energy and concentrates it on the receivers, which are positioned at the parabola's center. This procedure is depicted in diagram form in Fig. 1a. A heat exchanger flows through the receiver tube, transferring the photovoltaic solar energy to the fluid via temperature distribution. The fluid transports the usable energy to the diverse applications in which it is employed.

Bioconvection is known as a microorganism swimming in a particular direction that is heavier than water, resulting in a gradient of density that can contribute to the formation of a macroscopic convective motion. Bioconvection is a technique used in nanomaterials and bioengineering that has the potential to improve mass transport and induce mixing, especially in micro volumes that can be used to create a stable flow of nanofluids. As a result, primary-level bioconvection research in nanofluids may aid in the development of effective microfluid systems. Furthermore, bioconvection is crucial in mechanical engineering because the electrical field is understood to regulate the bioconvection phenomenon for the output of energy or mechanical power. Avramenko[34]

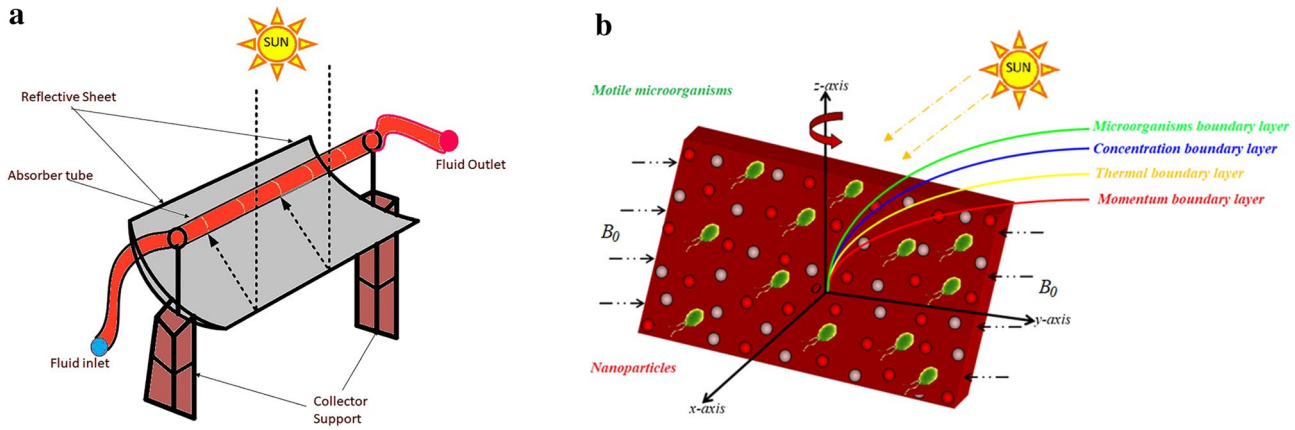

Figure 1. (**a**) Solar effects. (**b**) Physical sketch of the problem.

observed bioconvection when suspending miniature life forms. Bees et al.[35] investigated "bioconvection", which depicts hydrodynamic unsteadiness and examples of living body liquids. Khan et al.[36] examined the logical formation of silver nanoparticles over a given base liquid and the resulting nanofluids that create the base liquids' warmth limit. Tlili et al.[37] investigated the slip and activation-energy activities of Oldroyd-B nanofluids during bioconvection. Hassan et al.[38] investigated statistical mechanisms for transferring nanomaterials in liquid on a rotating disc with slip impacts. Shafiq et al.[39] investigated the bioconvection properties of a nanofluid under convective flow. Khan et al.[40] investigated the bioconvection consequences of nanoliquid. The capacity of charged digression magnetic nanofluids to engage with motile microorganisms was explored by Wang et al.[41]. The movement of tangent hyperbolic boundary layer flow microorganisms with bioconvection processes was studied by Shafiq et al.[42]. Khan et al.[43] used an oscillatory stretchy layer to examine the relevance of nanofluid bioconvection motion. The study of motile microorganisms, such as their movement variations, is based on their reactions to various science, industrial, fiscal, and social elements. More work on bioconvection is carried out[44–56].

The main purpose of the research is to investigate the effects of bioconvection and thermal radiation in the 3D flow of a viscoelastic nanofluid containing motile microorganisms above a stretching surface. The incorporation of motile microorganisms into nanomaterials is critical for increasing the thermal performance of a wide range of structures, including bacterial energy units, chemical biosensors, and bio-micro processes. The problem was discussed in terms of partial differential equations with suitable boundary conditions, which were then converted into a set of partial differential equations with non-similar variables. This provides control of PDEs was numerically solved using local non-similarity and the bvp4c shooting method. Graphs have been used to evaluate the aspect of the critical parameters on the flow field. Physical quantities including skin friction, local Sherwood, the local Nusselt, and the local motile microorganism number are tabulated with different physical parameter values. The ranges of the physical flow parameters like as $0.5 \leq \mathrm{Pr} \leq 2.0, 0.1 \leq Rd \leq 1.5, 0.0 \leq \alpha \leq 1.2, 0.2 \leq \gamma_1 \leq 0.8, 0.5 \leq Nb \leq 2.0, 0.5 \leq Nt \leq 2.0, 0.1 \leq Nr \leq 1.5, 0.1 \leq Nc \leq 1.2, 0.1 \leq \lambda \leq 1.2, 0.0 \leq S \leq 0.6, 1.0 \leq Le \leq 2.0, 0.2 \leq \gamma_2 \leq 0.8, 0.1 \leq \beta \leq 1.5, 0.2 \leq \gamma_3 \leq 0.8, 0.1 \leq \mathrm{Pe} \leq 1.0$ and $1.0 \leq Lb \leq 2.0$ are discussed.

Mathematical formulation. Here we investigated the significance of Brownian motion, thermophoresis effects, and thermal radiation over a three-dimensional viscoelastic fluid containing swimming motile microorganisms over a stretched surface. For nanofluid, the Buongiorno model is being investigated. The bioconvection phenomenon is taken into account. We use a Cartesian coordinate system with extended x and y-axis coordinates and a z-axis perpendicular to the surface (see Fig. 1b). The stretching surface velocities along x the axis and y axis are introduced as $U_w(x) = \frac{ax}{1-ct}$ & $V_w(y) = \frac{by}{1-ct}$ respectively.

The flow equations are defined as

$$\left.\begin{aligned} &\nabla \cdot V = 0, \\ &\rho_f V_t = -\rho_f V \cdot \nabla V - \nabla p + \nabla.\sigma \\ &(\rho c_p)(T_t + V \cdot \nabla T) = \alpha_m \nabla^2 T + \tau\left(D_B \nabla T \cdot \nabla C + \tfrac{D_T}{T_\infty} \nabla T \cdot \nabla T\right) - 1/(\rho c)_f D_z q_r \\ &(\rho c_p)(C_t + V \cdot \nabla C) = D_B \nabla^2 C + \left(\tfrac{D_T}{T_\infty}\right) \nabla^2 T, \end{aligned}\right\}, \tag{1}$$

$$N_t + V \cdot \mathrm{J}_0 = 0, \tag{2}$$

where

$$\begin{aligned} &J_0 = NV + N\hat{V} - D_m \nabla N, \\ &\textit{where} \\ &\hat{V} = \left(bW_c/\Delta C\right) \nabla C. \end{aligned} \tag{3}$$

In which (V) is velocity vector, (α_m) is thermal diffusivity, (J_0) is the convection of liquid, and $\left(\hat{V}\right)$ cell swimming speed. Under considered assumptions, governing expressions related to conservations of mass, momentum, energy, volumetric concentration, and motile micro-organisms are described into following relations[12,39]:

$$u_x + v_y + w_z = 0, \tag{4}$$

$$\begin{aligned} u_t + uu_x + vu_y + wu_y = {} & \nu u_{zz} + k_0(u_{zzt} + uu_{zzx} + wu_{zzz} - u_x u_{zz} - u_z w_{zz} - 2u_z u_{xz} - 2w_z u_{zz}) \\ & + \frac{1}{\rho_f}\left[\left(1 - C_f\right)\rho_f \beta^{**}(T - T_\infty) - \left(\rho_p - \rho_f\right)g^*(C - C_\infty) - (N - N_\infty)g^*\gamma\left(\rho_m - \rho_f\right)\right], \end{aligned} \tag{5}$$

$$v_t + uv_x + vv_y + wv_z = \nu v_{zz} + k_0\left(v_{zzt} + vv_{zzy} + wv_{zzz} - v_y v_{zz} - v_z w_{zz} - 2v_z v_{yz} - 2w_z v_{zz}\right), \tag{6}$$

$$T_t + uT_x + vT_y + wT_z = \alpha T_{zz} + \frac{(\rho c)_p}{(\rho c)_f}\left(D_B(T_z C_z) + \frac{D_T}{T_\infty}(T_z)^2\right) - \frac{1}{\rho c_p}\left(q_r\right)_z, \tag{7}$$

$$C_t + uC_x + vC_y + wC_z = D_B(C_{zz}) + \frac{D_T}{T_\infty}(T_{zz}), \tag{8}$$

$$N_t + uN_x + vN_y + wN_z + \frac{bW_c}{(C_w - C_\infty)}[\partial_z(NC_z)] = D_m \partial_z(N_z). \tag{9}$$

The radiative heat flux is expressed as

$$q_r = -\frac{4\sigma^*}{3k^*}D_z T^4 = -\frac{16\sigma^*}{3k^*}T^3(D_z T). \tag{10}$$

Then expression (7) becomes

$$T_t + uT_x + vT_y + wT_z = \alpha_m T_{zz} + \frac{(\rho c)_p}{(\rho c)_f}\left(D_B(T_z C_z) + \frac{D_T}{T_\infty}(T_{zz})^2\right) + \frac{1}{\rho c_p}\frac{16\sigma^*}{3k^*}\partial_z\left(T^3 T_z\right). \tag{11}$$

The subjected boundary constraints are

$$\left.\begin{array}{l} u = U_w = \frac{ax}{1-ct},\ v = V_w = \frac{by}{1-ct},\ w = 0,\ -k\,T_z = h_f(T_w - T),\ -D_B C_z = h_g(C_w - C), \\ -D_m N_z = h_m(N_w - N)\,, at\ z = 0,\ T_w = T_0 + a_1^* x, C_w = C_0 + a_2^* x, N_w = N_0 + a_3^* x, \\ u \to 0,\ v \to 0,\ T = T_0 + d_1^* x,\ C = C_0 + d_2^* x,\ N = N_0 + d_3^* x,\ as\ z \to \infty, \end{array}\right\}. \tag{12}$$

In expressions (4)-(12), the components along x, y, and z axes are denoted as u , v and w respectively, $\left((\rho c)_p\right)$ the heat capacity of nanoparticles, $\left(\rho_f\right)$ is the fluid density, (ρ_m) density of microorganisms, (β^{**}) volumetric expansion of the liquid, (μ) dynamic viscosity, $\left(\nu = \frac{\mu}{\rho_f}\right)$ kinematic viscosity, $\left((\rho c)_f\right)$ heat capacity of base fluid, (γ) the average volume of the microorganisms, $\left(q_r\right)$ radiative heat flux, $\left(\rho_f\right)$ density of the base fluid, (σ^*) Stephan Boltzmann constant, (k^*) absorption coefficient, (N) microorganisms, (N_w, N_∞) microorganisms surface and microorganisms away from surface respectively, $\left(a_1^*, a_2^*, a_3^*, d_1^*, d_2^*, d_3^*\right)$ are dimensionless constants, $\left(g^*\right)$ is gravity, $\left(\alpha_m = \frac{k}{(\rho_f)_f}\right)$ is thermal diffusivity, (T) temperature, $\left(k_0 = \frac{\alpha_1}{\rho_f}\right)$ is viscoelastic fluid constant, (C) nanoparticles concentration, (T_w) wall temperature, (T_∞) temperature at surface (D_B), (D_T) and (D_m) are Brownian motion, thermophoresis effects and microorganisms diffusions respectively (C_w) is the concentration at the stretchable sheet and (C_∞) is the concentration of nanofluid away from the surface.

To obtain the dimensionless forms of Eqs. (4)-(12), the following similarities are tested[12,39]:

$$\left.\begin{array}{l} u = \frac{ax}{(1-ct)}f'(\zeta),\ v = \frac{ay}{(1-ct)}g'(\zeta),\ w = -\sqrt{\frac{a\nu}{(1-ct)}}\left(f(\zeta) + g(\zeta)\right), \zeta = \sqrt{\frac{a}{\nu(1-ct)}}\mathrm{z}, \\ \theta(\zeta)(T_w - T_\infty) + T_\infty = T,\ \phi(\zeta)(C_w - C_\infty) + C_\infty = C,\ \chi(\zeta)(N_w - N_\infty) + N_\infty = N, \end{array}\right\}. \tag{13}$$

The results of main equations are

$$\begin{aligned} & f''' - f'^2 - S\left(\frac{\zeta}{2}f'' + f'\right) + (f+g)f'' - \beta\left(\begin{array}{l} -S\left(\frac{\zeta}{2}f^{iv} + 2f'''\right) + (f+g)f^{iv} \\ +(f'' + g'')f'' - 2(f' + g')f''' \end{array}\right) \\ & \quad + \lambda[\theta - Nr\phi - Nc\chi] = 0, \end{aligned} \tag{14}$$

$$g''' - g'^2 - S\left(\frac{\zeta}{2}f'' + f'\right) + (f+g)g'' - \beta\begin{pmatrix} -S\left(\frac{\zeta}{2}g^{iv} + 2g'''\right) + (f+g)g^{iv} \\ +(g''-f'')g'' - 2(f'+g')g''' \end{pmatrix} = 0, \tag{15}$$

$$\left(1+\frac{4}{3}Rd\right)\theta'' + Pr\left((f+g)\theta' - f'\theta - S_1 f' + Nb\theta'\phi' + Nt\theta'^2 - S\left(\frac{\zeta}{2}\theta' - \theta\right)\right) = 0, \tag{16}$$

$$\phi'' + LePr\left((f+g)\phi' - f'\phi - S_2 f' - S\left(\frac{\zeta}{2}\phi' - \phi\right)\right) + \left(\frac{Nt}{Nb}\right)\theta'' = 0, \tag{17}$$

$$\chi'' + Lb\chi'(f+g) - LbS_3 f' - Pe\left[\phi''(\chi+\delta_1) + \chi'\phi'\right] = 0, \tag{18}$$

with

$$\left.\begin{array}{l} f(0)=0,\, g(0)=0,\, f'(0)=1,\, g'(0)=\alpha,\, \theta'(0)=-\gamma_1(1-S_1-\theta(0)), \\ \phi'=-\gamma_2(1-S_2-\phi(0)),\, \chi'=-\gamma_3(1-S_3-\chi(0)),\, at\ \zeta\to 0, \\ f'\to 0,\, g'\to 0,\, \theta\to 0,\, \phi\to 0,\, \chi\to 0,\, as\ \zeta\to\infty \end{array}\right\}, \tag{19}$$

where (S) unsteadiness parameter, (β) viscoelastic fluid parameter, (Nr) buoyancy parameter, (Nc) bio-convection Rayleigh parameter,(λ) mixed convective number,(Nt) thermophoresis parameter, (α) ratio parameter,(Nb) Brownian motion number,(Le) Lewis number,(Rd) radiation parameter,(Pr) Prandtl parameter,(δ_1) microorganisms concentration difference number,(Lb) bioconvection Lewis number,(Pe) Peclet number,(γ_1) thermal Biot parameter, (γ_2) solutal Biot parameter, (γ_3) stratification Biot number,(S_1) thermally stratified parameter,(S_2) solutal stratified variable, and (S_3) motile stratification number which are mathematically related in following forms:

$$\left.\begin{array}{l} S\left(=\frac{c}{a},\right)\beta\left(=\frac{K_0 a}{\nu(1-ct)}\right), Nr\left(=\frac{(\rho_p-\rho_f)(C_w-C_\infty)}{(T_w-T_\infty)\beta^{**}\rho_f(1-C_\infty)}\right), \alpha\left(=\frac{b}{a}\right), Le\left(=\frac{\alpha_m}{D_B}\right), \\ Nc\left(=\frac{\gamma(\rho_m-\rho_f)(N_w-N_\infty)}{\rho_f(1-C_\infty)(T_w-T_\infty)\beta^{**}}\right),\ \lambda\left(=\frac{\beta^{**}g^*(T_w-T_\infty)(1-C_\infty)(1-ct)^2}{a^2 x}\right), \\ Nt\left(=\frac{(\rho c)_p D_T(T_w-T_\infty)}{(\rho c)_f T_\infty \nu}\right),\ Nb\left(=\frac{(\rho c)_p D_B(C_w-C_\infty)}{(\rho c)_f \nu}\right), Rd\left(=\frac{4\sigma^* T_\infty^3}{kk^*}\right), \\ \mathrm{Pr}\left(=\frac{\nu}{\alpha_m}\right), \delta_1\left(=\frac{N_\infty}{N_w-N_\infty}\right), \mathrm{Lb}\left(=\frac{\nu}{D_m}\right), Pe\left(=\frac{bW_c}{D_m}\right), \gamma_1\left(=\left(\frac{h_f}{k}\right)\sqrt{\frac{\nu(1-ct)}{a}}\right), \\ \gamma_2\left(=\left(\frac{h_g}{k}\right)\sqrt{\frac{\nu(1-ct)}{a}}\right), \gamma_3\left(=\left(\frac{h_m}{k}\right)\sqrt{\frac{\nu(1-ct)}{a}}\right), S_1\left(=\frac{d_1^*}{a_1^*}\right), S_2\left(=\frac{d_2^*}{a_2^*}\right), S_3\left(=\frac{d_3^*}{a_3^*}\right) \end{array}\right\}. \tag{20}$$

The physical quantities such as Nusselt number is introduced as[5,12–57].

$$Nu_x = -\frac{x}{(T-T_\infty)}\frac{\partial T}{\partial z}\bigg|_{z=0}. \tag{21}$$

Sherwood number and microorganism's density number are addressed as

$$\begin{aligned} \mathrm{Sn}_x &= \frac{x j_m}{D_T(C_w - C_\infty)}, \\ \mathrm{Nn}_x &= \frac{x j_n}{D_m(N_w - N_\infty)}. \end{aligned} \tag{22}$$

From above relations (21) and (22), we obtain the following dimensionless forms:

$$\begin{aligned} \mathrm{Re}^{\frac{-1}{2}} Nu &= -\theta'(0), \\ \mathrm{Re}^{\frac{-1}{2}} Sn &= -\theta'(0), \\ Nn\mathrm{Re}_x^{-\frac{1}{2}} &= -\chi'(0). \end{aligned} \tag{23}$$

The local Reynolds number is $\mathrm{Re} = \frac{ux}{\nu}$.

Numerical approach. Because of its accuracy and performance, the bvp4c scheme numerically computes the expressions (14)-(18) with boundary conditions (19). Initially, coupled non-linear ODEs are converted to first-order initial-value problems using the following procedure:

$$\left.\begin{array}{l} f = z_1, f' = z_2, f'' = z_3, f''' = z_4, f^{iv} = z_4', \mathrm{g} = z_5, \mathrm{g}' = z_6, \\ \mathrm{g}'' = z_7, \mathrm{g}''' = z_8, \mathrm{g}^{iv} = z_8', \theta = z_9, \theta' = z_{10}, \theta'' = z_{10}', \phi = z_{11}, \\ \phi' = z_{12}, \phi'' = z_{12}', \chi = z_{13}, \chi' = z_{14}, \chi'' = z' z_{14}' \end{array}\right\} \tag{24}$$

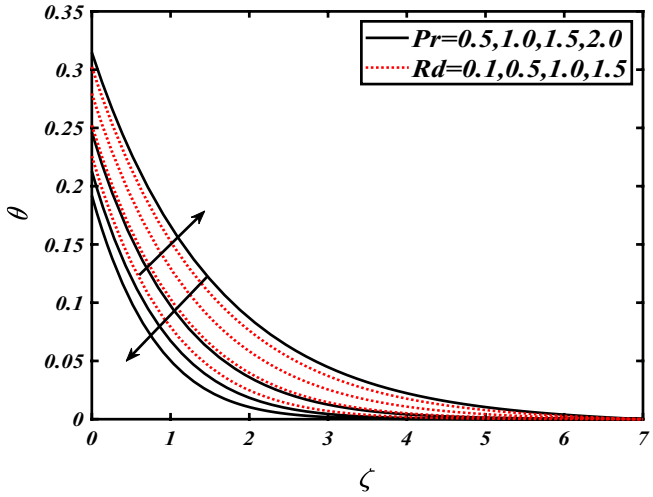

Figure 2. Illustration of *Pr and Rd* over-temperature θ when $\alpha = 0.5, Nb = 0.2, Nt = 0.3, S = 0.5, \lambda = 0.5, \beta = 0.2$.

$$
\left.
\begin{aligned}
& -z_4 + z_2^2 + S(0.5\zeta z_3 + z_2) - (z_1 + z_5)z_3 + \beta \begin{pmatrix} -2Sz_4 + (z_3 + z_7)z_3 \\ -2(z_2 + z_6)z_4 \end{pmatrix} \\
z_4^{'} &= \frac{-\lambda[z_9 - Nrz_{11} - Ncz_{13}]}{\beta(S(0.5\zeta) - (z_1 + z_5))}, \\
& -z_8 + z_6^2 + S(0.5\zeta z_3 + z_2) - (z_1 + z_5)z_7 + (z_7 - z_3)z_7 - 2(z_2 + z_6)z_8 \\
& + \beta \begin{pmatrix} -2sz_8 + (z_7 + z_3)z_7 \\ -2(z_2 - z_6)z_8 \end{pmatrix} \\
z_8^{'} &= \frac{}{\beta(S(0.5\zeta) - (z_1 + z_5))}, \\
z_{10}^{'} &= -Pr\big((z_1 + z_5)z_{10} - z_2 z_9 - S_1 z_2 + Nbz_{10}z_{12} + Ntz_{10}^2 - S(0.5\zeta z_{10} - z_9)\big), \\
z_{12}^{'} &= -Le\,\mathrm{Pr}\,((z_1 + z_5)z_{12} - z_2 z_{11} - S_2 z_2 - S(0.5\zeta z_{12} - z_{11})) + \left(\tfrac{Nt}{Nb}\right)z_{10}^{'}, \\
z_{14}^{'} &= Pe\left[z_{12}^{'}(z_{13} + \delta_1) + z_{12}z_{14}\right] - Lbz_1 z_{14} + LbS_3 z_2, \\
& z_1(0) = 0,\ z_5(0) = 0,\ z_2(0) = 1,\ z_6(0) = \alpha,\ z_{10}(0) = -\gamma_1(1 - S_1 - z_9(0)), \\
& z_{12} = -\gamma_2(1 - S_2 - z_{11}(0)), z_{14} = -\gamma_3(1 - S_3 - z_{13}(0)),\ at\ \zeta \to 0, \\
& z_2 \to 0,\ z_6 \to 0,\ z_9 \to 0,\ z_{11} \to 0,\ z_{13} \to 0, as\ \zeta \to \infty
\end{aligned}
\right\}. \tag{25}
$$

Results and discussion

In the present section, our prime motive is to scrutinize the physical influence of the numerical model through graphical illustrations. The rheological behavior of significant parameters like radiation parameter *Rd*, viscoelastic fluid parameter β, unsteady parameter *S*, mixed convection parameter λ, Lewis number *Le*, bioconvection Lewis number *Lb*, ratio parameter α, Peclet number *Pe*, Brownian motion parameter *Nb*, Prandtl number Pr, thermal boot number γ_1, buoyancy ratio parameter *Nr*, thermophoresis parameter *Nt*, solutal Biot number γ_2, bioconvection Rayleigh number *Nc* and stratification Biot number γ_3 for velocities, temperature, nanoparticles concentration, and motile microorganisms profiles is observed. The ranges of the different parameters like as,$0.1 \le Nc \le 1.2, 0.0 \le \alpha \le 1.2, 0.2 \le \gamma_1 \le 0.8, 0.0 \le S \le 0.6, 1.0 \le Le \le 2.0, 0.5 \le Nt \le 2.0, 0.5 \le \mathrm{Pr} \le 2.0, 0.1 \le Nr \le 1.5, 0.5 \le Nb \le 2.0, 0.1 \le \lambda \le 1.2, 0.1 \le Rd \le 1.5, 0.2 \le \gamma_2 \le 0.8, 0.2 \le \gamma_3 \le 0.8, 1.0 \le Lb \le 2.0$,$0.1 \le \beta \le 1.5$ and $0.1 \le \mathrm{Pe} \le 1.0$ are analyzed.

Thus Figs. 2, 3, 4, 5, 6, 7, 8, 9, 10, 11, 12, 13, 14 and 15 are drafted. The plot of temperature distribution $\theta(\zeta)$ for various variations Pr and *Rd* is portrayed in Fig. 2. It is analyzed that the rise of thermal radiation parameter *Rd* leads to an increment in temperature field $\theta(\zeta)$ and it is declining for Prandtl number Pr. Physically Pr is an inverse proportion to temperature. A larger Prandtl number Pr declines the thermal diffusivity which shows a decrement in the temperature of the fluid. Physically more heat is produced when thermal radiation is improved. The deteriorating behavior of the ratio parameter α and Biot number γ_1 against $\theta(\zeta)$ is delineated in Fig. 3. As anticipated, temperature distribution $\theta(\zeta)$ dwindles for progressive values of the ratio parameter α. Furthermore, the temperature distribution $\theta(\zeta)$ is boomed up by rising values of thermal Biot number γ_1.Physically by

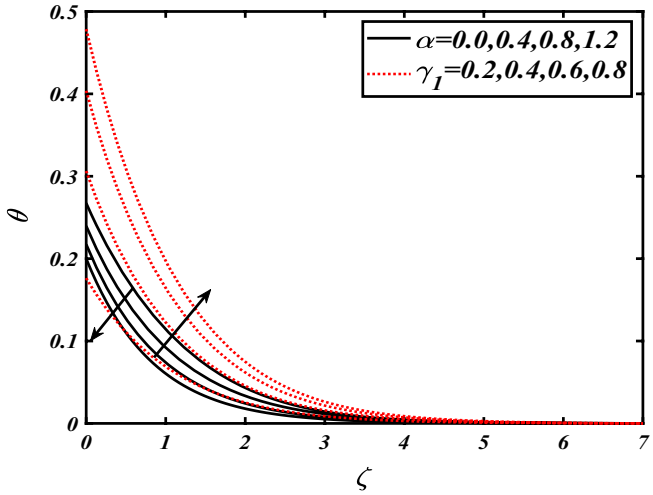

Figure 3. Illustration of α *and* γ_1 over-temperature θ when $Pr = 2.0, \mathrm{Rd} = 0.4, \gamma_2 = 0.3, Nb = 0.2, Nt = 0.3, S = 0.5, \lambda = 0.5, \beta = 0.2$.

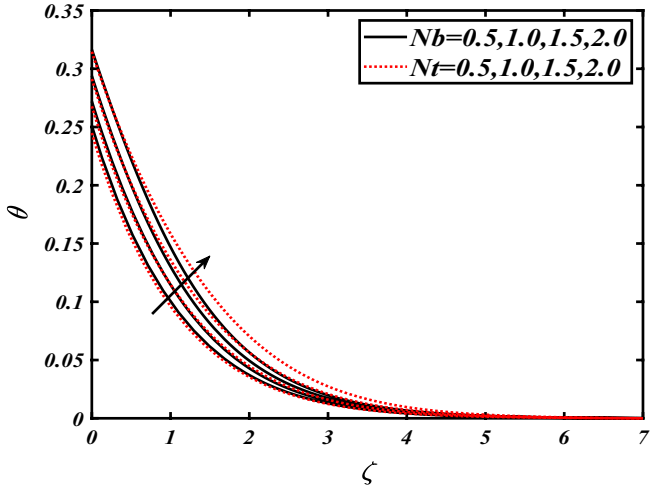

Figure 4. Illustration of *Nb and Nt* over-temperature θ when $Pr = 2.0, \mathrm{Rd} = 0.4, \gamma_2 = 0.3, Nr = 0.2, Nc = 0.2, S = 0.5, \lambda = 0.5, \beta = 0.2$.

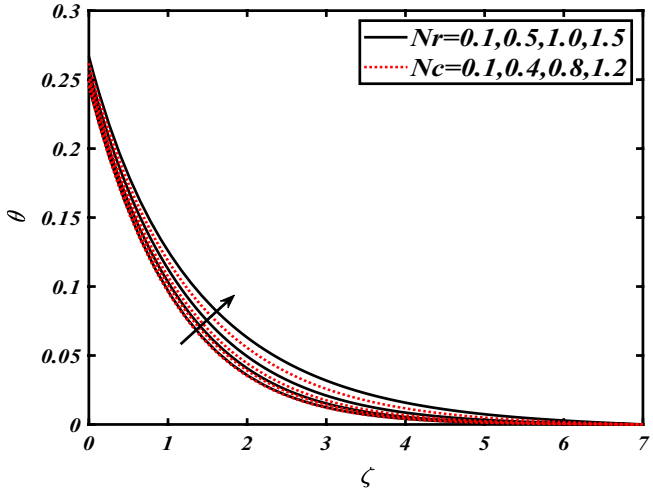

Figure 5. Illustration of *Nr and Nc* overtemperature θ when $Pr = 2.0, \mathrm{Rd} = 0.4, \gamma_2 = 0.3, Nb = 0.2, Nt = 0.3, S = 0.5, \lambda = 0.5, \beta = 0.2$.

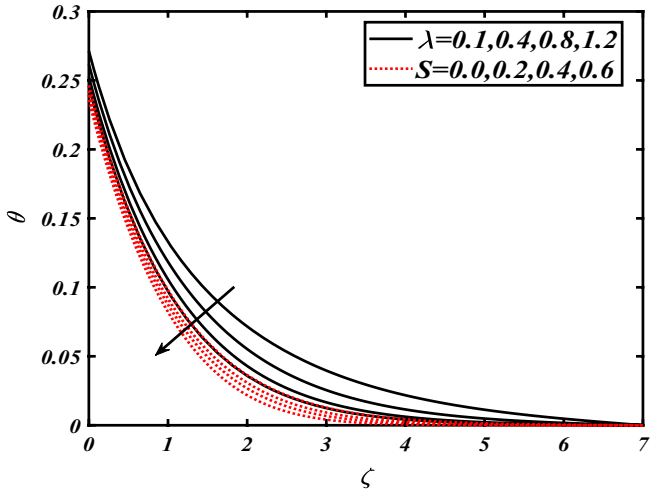

Figure 6. Illustration of λ *and* S over-temperature θ when $Pr = 2.0, \mathrm{Rd} = 0.4, \gamma_2 = 0.3, Nb = 0.2, Nt = 0.3, \beta = 0.2$.

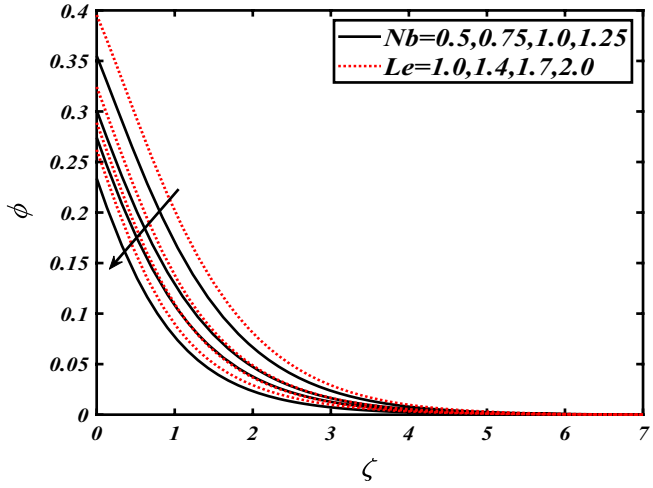

Figure 7. Illustration of *Nb and Le* over nanoparticles concentration ϕ when $Pr = 2.0, \mathrm{Rd} = 0.4, \gamma_2 = 0.3, \gamma_1 = 0.3, Nt = 0.3, S = 0.5, \lambda = 0.5, \beta = 0.2$.

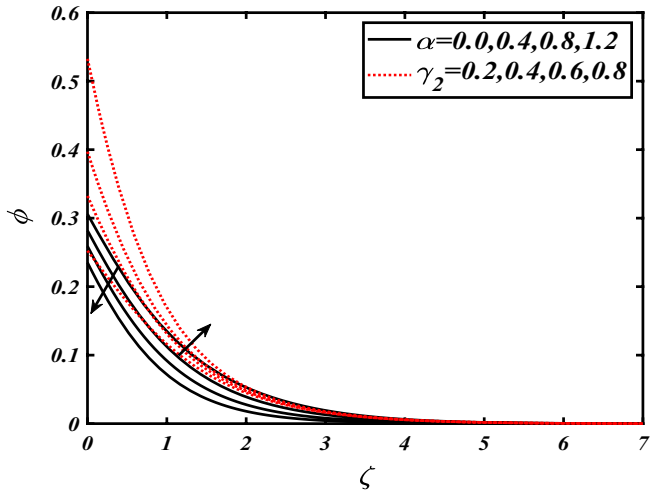

Figure 8. Illustration of α *and* γ_2 over nanoparticles concentration ϕ when $Pr = 2.0, \mathrm{Rd} = 0.4, \gamma_1 = 0.3, Nt = 0.3, S = 0.5, \lambda = 0.5, \beta = 0.2$.

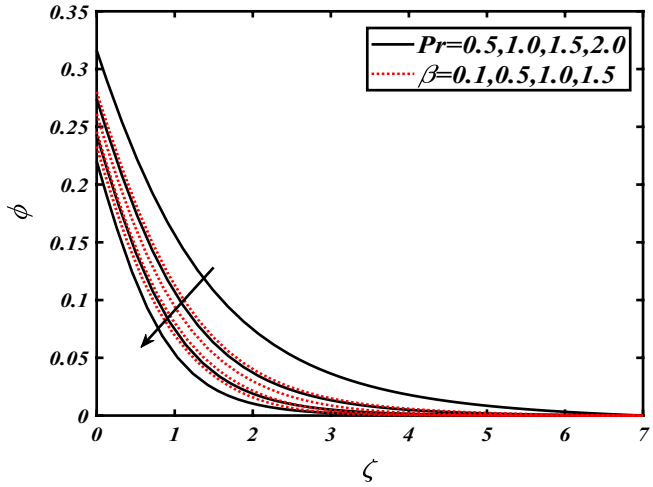

Figure 9. Illustration of Pr *and* β over nanoparticles concentration ϕ when Rd $= 0.4$, $\gamma_2 = 0.3$, $\gamma_1 = 0.3$, $Nt = 0.3$, Nb $= 0.2$, Nr $= 0.2$, $S = 0.5$, $\lambda = 0.5$.

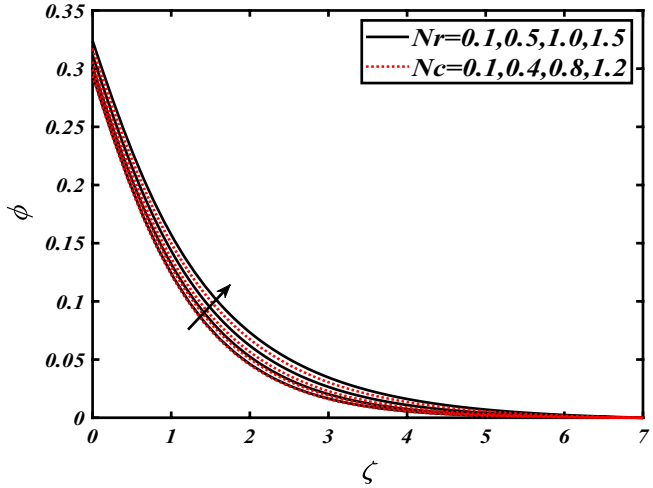

Figure 10. Illustration of *Nr and Nc* over nanoparticles concentration ϕ when Rd $= 0.4$, $\gamma_2 = 0.3$, $\gamma_1 = 0.3$, $Nt = 0.3$, Nb $= 0.2$, $S = 0.5$, $\lambda = 0.5$.

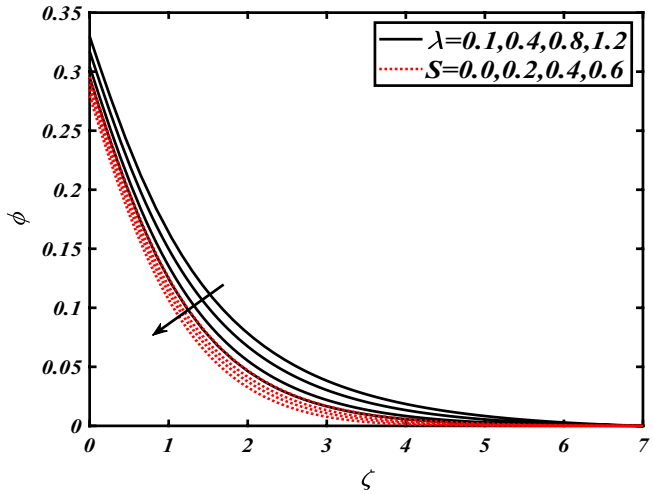

Figure 11. Illustration of λ *and* S over nanoparticles concentration ϕ when Rd $= 0.4$, $\gamma_2 = 0.3$, $\gamma_1 = 0.3$, $Nt = 0.3$, Nb $= 0.2$, Nr $= 0.2$.

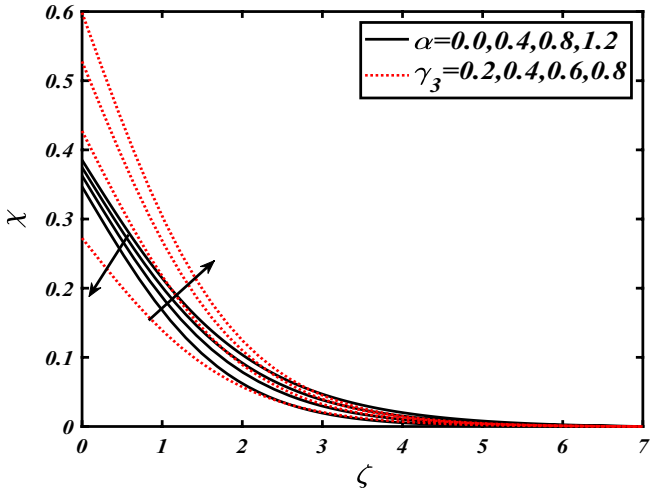

Figure 12. Illustration of α *and* γ_3 over motile microorganisms χ when Rd $= 0.4, \gamma_2 = 0.3, \gamma_1 = 0.3,$ $Nt = 0.3$, Nb $= 0.2$, Nr $= 0.2, S = 0.5, \lambda = 0.5$, Pe $= 0.1$, Lb $= 2.0$.

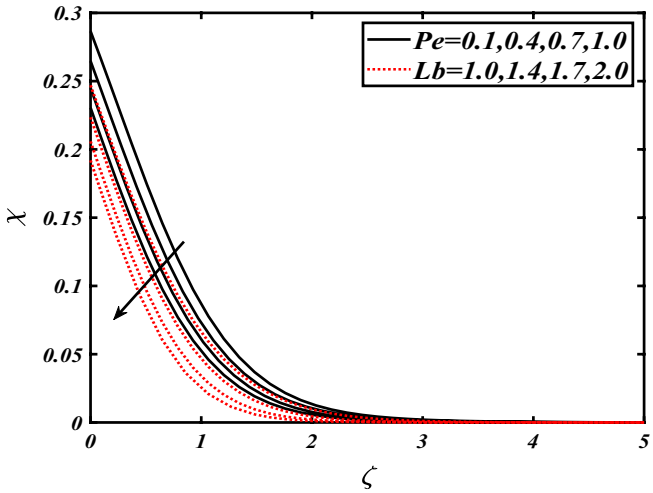

Figure 13. Illustration of *Pe and Lb* over motile microorganisms χ when Rd $= 0.4, \gamma_2 = 0.3, \gamma_1 = 0.3,$ $Nt = 0.3$, Nb $= 0.2$, Nr $= 0.2, S = 0.5, \lambda = 0.5$.

increasing the values of thermal Biot number reduces the resistance for energy transport at the surface and as a result, more temperature is attained. Figure 4 intimates the illustration of *Nb* and thermophoresis parameter *Nt* via $\theta(\zeta)$. The temperature field $\theta(\zeta)$ is progressive for higher values of both parameters (Brownian motion parameter *Nb*&thermophoresis parameter *Nt*). Brownian movement is the random movement of fluid suspended molecules caused by a collision with the rapidly moving particles of the fluid. Physically in thermophoresis mechanisms i.e., the particles of fluid transport from a hot region to a cool region. The behavior of buoyancy ratio parameter *Nr* and bioconvection Rayleigh number *Nc* over-temperature filed $\theta(\zeta)$ is demonstrated in Fig. 5. In the current situation for higher variations of *Nr* and bioconvection Rayleigh number *Nc*, temperature $\theta(\zeta)$ increases. Figure 6 discloses the roles of unsteady parameter *S* and mixed convection parameter λ versus thermal distribution $\theta(\zeta)$. The temperature distribution $\theta(\zeta)$ is truncated subjected to the higher deviation of λ and unsteady number *S*. Figure 7 communicates the physical significance of the *Nb* and *Le* against concentration $\phi(\zeta)$. Contrasting behavior is observed in volumetric concentration $\phi(\zeta)$ against Lewis number *Le* and Brownian motion parameter *Nb*. Physically enhancing values of Lewis number reduces the mass diffusivity. Thus energy profile diminishes. Figure 8 elucidates the influence of ratio parameter α and solutal Biot number γ_2 against volumetric concentration $\phi(\zeta)$. It is intimated that due to increment in solutal Biot number γ_2 the volumetric concentration $\phi(\zeta)$ is enhanced. Furthermore, we observed that the concentration curves also decreased for enhancement in the ratio parameter α. The consequences of Pr and viscoelastic fluid parameter β on volumetric concentration $\phi(\zeta)$ are communicated in Fig. 9. It is noted that the $\phi(\zeta)$ reduces by uplifting the variations of Prandtl number Pr and viscoelastic parameter β. Figure 10 is captured the vital role of bioconvection Rayleigh number *Nc* and buoyancy ratio parameter *Nr* via concentration field $\phi(\zeta)$. The concentration field

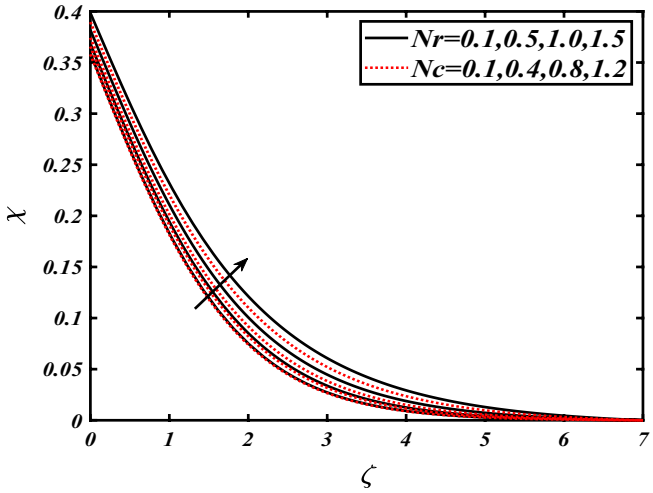

Figure 14. Illustration of *Nr and Nc* over motile microorganisms χ when Rd $= 0.4, \gamma_2 = 0.3, \gamma_1 = 0.3,$ Nr $= 0.2, S = 0.5, \lambda = 0.5,$ Pe $= 0.1,$ Lb $= 2.0$.

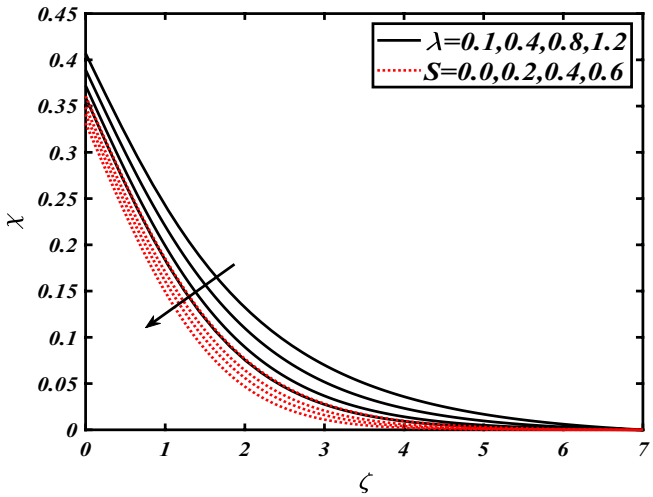

Figure 15. Illustration of λ *and S* over motile microorganisms χ when Rd $= 0.4, \gamma_2 = 0.3, \gamma_1 = 0.3,$ Nr $= 0.2,$ Pe $= 0.1,$ Lb $= 2.0$.

$\phi(\zeta)$ is knocked down due to progressive values of buoyancy ratio parameter *Nr* and bioconvection Rayleigh number *Nc*. Figure 11 determines the inspiration of λ an unsteady number *S* on volumetric concentration $\phi(\zeta)$. A retarded concentration has been examined with the variation of mixed convection parameter λ and unsteady number *S*. It can be seen that the concentration declines with an enhancing mixed convection parameter λ. The concentration field also reduces for different variations of the unsteady parameter *S*. Figure 12 constitutes the outcomes of mixed convection parameter λ and stratification Biot number γ_3 on $\chi(\zeta)$. The motile microorganism $\chi(\zeta)$ upsurges by varying values of stratification Biot number γ_3. The curve of motile microorganisms $\chi(\zeta)$ maps down for growing mixed convection parameter λ. Figure 13 is mapped to delineate the significance of Peclet number Pe and bioconvection Lewis number *Lb* over motile microorganism's concentration $\chi(\zeta)$. Motile microorganism's field $\chi(\zeta)$ diminishes when the Peclet number Pe enhances. Furthermore, a decreasing trend is noted by variations of bioconvection Lewis number *Lb*.Physically, when we enhance the Peclet number Pe, the diffusion of microorganisms reduces which causes a reduction in the microorganism's profile. Figure 14 reports the diversity of motile microorganisms field $\chi(\zeta)$ for several estimations of buoyancy ratio parameter *Nr* and bioconvection Rayleigh number *Nc*. Improvement in both parameters divulges the enhancing conduct for motile microorganisms $\chi(\zeta)$. Figure 15 depicts a variety of mixed convective parameter λ and unsteady number *S* against motile microorganisms. Interestingly motile microorganisms $\chi(\zeta)$ are declining function for mixed convection parameter λ and unsteady parameter *S*.To illustrate the inspiration of prominent flow parameters versus local Nusselt and Sherwood numbers, Table 1 is captured. The features of the involved parameters are deeply analyzed. Local Sherwood and Nusselt numbers are enhanced by growing variation of Prandtl number Pr. The performance of prominent parameters against the density of motile microorganisms is divulged in Table 2. It is analyzed that

S	β	Pr	Nb	Nt	Le	λ	Nr	Nc	γ_1	$-\theta'(0)$	$-\phi'(0)$
1.0	0.0	1.2	0.2	0.3	2.0	0.1	0.2	0.2	0.3		
0.1 0.4 0.8	0.0	1.2	0.2	0.3	2.0	0.1	0.2	0.2	0.3	0.2406 0.2434 0.2480	0.2532 0.2520 0.2518
1.0	0.0 0.4 0.8	1.2	0.2	0.3	2.0	0.1	0.2	0.2	0.3	0.2497 0.2503 0.2508	0.2515 0.2523 0.2529
1.0	0.0	1.0 2.0 3.0	0.2	0.3	2.0	0.1	0.2	0.2	0.3	0.2461 0.2595 0.2660	0.2486 0.2609 0.2673
1.0	0.0	1.2	0.1 0.4 0.8	0.3	2.0	0.1	0.2	0.2	0.3	0.2503 0.2495 0.2485	0.2343 0.2607 0.2650
1.0	0.0	1.2	0.2	0.1 0.5 1.0	2.0	0.1	0.2	0.2	0.3	0.2506 0.2494 0.2479	0.2634 0.2407 0.2138
1.0	0.0	1.2	0.2	0.3	1.0 1.4 1.8	0.1	0.2	0.2	0.3	0.2247 0.2297 0.2307	0.2344 0.2432 0.2494
1.0	0.0	1.2	0.2	0.3	2.0	0.2 0.4 0.8	0.2	0.2	0.3	0.2405 0.2513 0.2623	0.2513 0.2612 0.2714
1.0	0.0	1.2	0.2	0.3	2.0	0.1	0.3 0.4 0.5	0.2	0.3	0.2357 0.2349 0.2334	0.2515 0.2494 0.2448
1.0	0.0	1.2	0.2	0.3	2.0	0.1	0.2	0.3 0.4 0.5	0.3	0.2256 0.2149 0.2066	0.2442 0.2424 0.2401
1.0	0.0	1.2	0.2	0.3	2.0	0.1	0.2	0.2	0.1 0.5 1.0	0.0939 0.3740 0.5927	0.2628 0.2442 0.2303

Table 1. Tabulations of $-\theta'(0)$ and $-\phi'(0)$ with variations of α, S, β, Pr, Nb, Nt, Le, λ, Nr, Nc and γ_1.

S	β	λ	Nr	Nc	Pe	Lb	γ_3	$-\chi'(0)$
1.0	0.0	0.1	0.2	0.2	0.1	2.0	0.3	
0.1 0.4 0.8	0.0	0.1	0.2	0.2	0.1	2.0	0.3	0.2574 0.2567 0.2559
1.0	0.0 0.4 0.8	0.1	0.2	0.2	0.1	2.0	0.3	0.2554 0.2561 0.2565
1.0	0.0	0.2 0.4 0.8	0.2	0.2	0.1	2.0	0.3	0.2658 0.2743 0.2840
1.0	0.0	0.1	0.3 0.4 0.5	0.2	0.1	2.0	0.3	0.2635 0.2657 0.2701
1.0	0.0	0.1	0.2	0.3 0.4 0.5	0.1	2.0	0.3	0.2725 0.2653 0.2513
1.0	0.0	0.1	0.2	0.2	0.2 0.5 0.8	2.0	0.3	0.2547 0.2601 0.2628
1.0	0.0	0.1	0.2	0.2	0.1	1.0 1.4 1.8	0.3	0.2371 0.2466 0.2528
1.0	0.0	0.1	0.2	0.2	0.1	2.0	0.1 0.5 1.0	0.0948 0.3907 0.6408

Table 2. Tabulations of $-\chi'(0)$ with variations of α, S, β, λ, Nr, Nc, Pe, Lb and γ_3.

the density number of motile microorganisms shows the declining trend for higher variations of bioconvection Lewis number *Lb* and Peclet number Pe.

Conclusions

The physical representation of the three-dimensional time-dependent flow of viscoelastic nanofluid via a stretched surface in the presence of microorganisms has been examined. The viscoelastic fluid contains both elastic and viscous properties. Physical results of the various parameters are described by using different graphs. Volumetric fraction of nanoparticles and the temperature distribution are significantly retarded as mounting values of unsteadiness parameter while temperature and concentration profiles are elevated for the rising values of thermophoresis parameter. The concentration profile shows favorable reduction due to variation in Brownian motion parameter while the inverse pattern is observed for bioconvection Rayleigh number. The decreasing trend over-concentration of nanoparticles is to be noticed as intensifying values of the viscoelastic parameter. The volumetric concentration of nanoparticles reduces by boosting the Prandtl number. Increased bioconvection Lewis and Peclet populations decrease the motile microorganism field. In biomedicine and automobile solutions, electrochemistry, and mechanics, viscoelastic fluid play a vital role[58–60]. The significant applications in the fields of nanotechnology, bacteriology, bioengineering, petroleum, metalworking, biofuels, and engineering problems, for the research of nanofluid, has piqued the interest of researchers and scientist in recent years. The latest results are precise and pure, making them more useful in engineering fields.

Received: 7 September 2021; Accepted: 27 January 2022
Published online: 22 February 2022

References

1. Choi, S. U. S. & Eastman, J. A. Enhancing thermal conductivity of fluids with nanoparticles. In *Developments and Applications of Non-Newtonian Flows*, vol. 231 99–106 (ASME, 1995).
2. Buongiorno, J. Convective transport in nanofluids. *J. Heat Transf.* **128**, 240–250 (2006).
3. Hsiao, K. L. Micropolarnanofluid flow with MHD and viscous dissipation effects towards a stretching sheet with the multimedia feature. *Int. J. Heat Mass Transf.* **112**, 983–990 (2017).
4. Turkyilmazoglu, M. Buongiorno model in a nanofluid filled asymmetric channel fulfilling zero net particle flux at the walls. *J. Heat Mass Transf. Part A* **126**, 974–979 (2018).
5. Alblawi, A., Malik, M. Y., Nadeem, S. & Abbas, N. Buongiorno's nanofluid model over a curved exponentially stretching surface. *Processes* **7**, 665 (2019).
6. Khan, W. A. & Pop, I. Boundary-layer flow of a nanofluid past a stretching sheet. *Int. J. Heat Mass Transf.* **12**, 2477–2483 (2010).
7. Shafiq, A., Khan, I., Rasool, G., Sherif, E. S. & Sheikh, A. H. Influence of single-and multi-wall carbon nanotubes on magnetohydrodynamic stagnation point nanofluid flow over the variable thicker surface with concave and convex effects. *Mathematics* **8**, 104 (2020).
8. Hayat, T., Ullah, I., Waqas, M. & Alsaedi, A. MHD stratified nanofluid flow by slandering surface. *Phys. Scr.* **93**, 115701 (2018).
9. Hayat, T., Ijaz, M., Qayyum, S., Ayub, M. & Alsaedi, A. Mixed convective stagnation point flow of nanofluid with Darcy–Forchheimer relation and partial slip. *Results Phys.* **9**, 771–778 (2018).
10. Azam, M., Khan, M. & Alshomrani, A. S. Effects of magnetic field and partial slip on the unsteady axisymmetric flow of Carreau-nanofluid over a radially stretching surface. *Results Phys.* **7**, 2671–2682 (2017).
11. Elgazery, N. S. Nanofluids flow over a permeable unsteady stretching surface with a non-uniform heat source/sink in the presence of the inclined magnetic field. *J. Egypt. Math. Soc.* **27**, 1–26 (2019).
12. Ahmad, M., Muhammad, T., Ahmad, I. & Aly, S. Time-dependent 3D flow of viscoelastic nanofluid over an unsteady stretching surface. *Physica A Stat. Mech. Appl.* **8**, 124004 (2020).
13. Hayat, T., Aziz, A., Muhammad, T. & Alsaedi, A. Active and passive controls of 3D nanofluid flow by a convectively heated nonlinear stretching surface. *Phys. Scr.* **94**, 085704 (2019).
14. Asma, M., Othman, W. A., Muhammad, T., Mallawi, F. & Wong, B. R. Numerical study for the magnetohydrodynamic flow of nanofluid due to a rotating disk with binary chemical reaction and Arrhenius activation energy. *Symmetry* **11**, 1282 (2019).
15. Eid, M. R., Mahny, K. L., Dar, A. & Muhammad, T. Numerical study for Carreaunanofluid flow over a convectively heated nonlinear stretching surface with chemically reactive species. *Physica A Stat. Mech. Appl.* **540**, 123063 (2020).
16. Al-Bashir, A., Al-Dweri, M., Al-Ghandoor, A., Hammad, B. & Al-Kouz, W. Analysis of effects of solar irradiance, cell temperature, and wind speed on photovoltaic systems performance. *Int. J. Energy Econ. Policy* **10**(1), 353 (2020).
17. Sohail, M. *et al.* Computational exploration for the radiative flow of Sutterby nanofluid with variable temperature-dependent thermal conductivity and diffusion coefficient. *Open Phys.* **18**(1), 1073–1083 (2020).
18. Nader, N., Al-Kouz, W. & Al-Dahidi, S. Assessment of existing photovoltaic system with cooling and cleaning system: A case study at Al-Khobar city. *Processes* **8**(1), 9 (2020).
19. Hussien, A. A., Al-Kouz, W., Yusop, N. M., Abdullah, M. Z. & Janvekar, A. A. A brief survey of preparation and heat transfer enhancement of hybrid nanofluids. *Strojniski Vestnik/J. Mech. Eng.* **65** (2019).
20. Abu-Libdeh, N. *et al.* Hydrothermal and entropy investigation of Ag/MgO/H2O hybrid nanofluid natural convection in a novel shape of the porous cavity. *Appl. Sci.* **11**(4), 1722 (2021).
21. Hussien, A. A. *et al.* Heat transfer and entropy generation abilities of MWCNTs/GNPs hybrid nanofluids in microtubes. *Entropy* **21**(5), 480 (2019).
22. Al-Kouz, W., Swain, K., Mahanthesh, B. & Jamshed, W. Significance of exponential space-based heat source and inclined magnetic field on heat transfer of hybrid nanoliquid with homogeneous-heterogeneous chemical reactions. *Heat Transf.* **50**(4), 4086–4102 (2021).
23. Mahesh, A. *et al.* Significance of non-Fourier heat flux and radiation on PEG-Water-based hybrid Nanofluid flow among revolving disks with chemical reaction and entropy generation optimization. *Int. Commun. Heat Mass Transf.* **127**, 105572 (2021).
24. Mahanthesh, B., Mackolil, J., Radhika, M. & Al-Kouz, W. Significance of quadratic thermal radiation and quadratic convection on boundary layer two-phase flow of a dusty nanoliquid past a vertical plate. *Int. Commun. Heat Mass Transf.* **120**, 105029 (2021).
25. Owhaib, W., Basavarajappa, M. & Al-Kouz, W. Radiation effects on the 3D rotating flow of Cu-water nanoliquid with viscous heating and prescribed heat flux using modified Buongiorno model. *Sci. Rep.* **11**(1), 1–16 (2021).
26. Hayat, T., Mumtaz, M., Shafiq, A. & Alsaedi, A. Stratified magnetohydrodynamic flow of tangent hyperbolic nanofluid induced by the inclined sheet. *Appl. Math. Mech.* **38**, 271–288 (2017).
27. Waqas, H., Muhammad, T., Noreen, S., Farooq, U. & Alghamdi, M. Cattaneo-Christov heat flux and entropy generation on hybrid nanofluid flow in a nozzle of a rocket engine with melting heat transfer. *Case Stud. Thermal Eng.* **28**, 101504 (2021).

28. Hussain, A. & Nadeem, S. MHD oblique stagnation point flow of copper-water nanofluid with variable properties. *Phys. Scr.* **94**, 125808 (2019).
29. Waqas, H., Farooq, U., Naseem, R., Hussain, S. & Alghamdi, M. Impact of MHD radiative flow of hybrid nanofluid over a rotating disk. *Case Stud. Thermal Eng.* **26**, 101015 (2021).
30. Ellahi, R., Sait, S. M., Shehzad, N. & Mobin, N. Numerical simulation and mathematical modeling of electro-osmotic Couette–Poiseuille flow of MHD power-law nanofluid with entropy generation. *Symmetry* **11**, 1038 (2019).
31. Nazari, S. *et al.* Numerical study on mixed convection of a non-Newtonian nanofluid with porous media in a two lid-driven square cavity. *J. Therm. Anal. Calorim.* **1**, 1–25 (2019).
32. Nadeem S, Abbas N. Effects of MHD on modified nanofluid model with variable viscosity in a porous medium. In *Nanofluid Flow in Porous Media*, vol. 7 (2019).
33. Hassan, M., Marin, M., Alsharif, A. & Ellahi, R. Convective heat transfer flow of a nanofluid in a porous medium over wavy surface. *Phys. Lett. A* **382**, 2749–2753 (2018).
34. Kuznetsov, A. V. & Avramenko, A. A. Effect of small particles on this stability of bioconvection in a suspension of gyrotactic microorganisms in a layer of finite depth. *Int. Commun. Heat Mass Transf.* **31**, 1 (2004).
35. Bees, M. A. Advances in Bioconvection. *Annu. Rev. Fluid Mech.* **52**, 449–476 (2020).
36. Khan, M., Irfan, M., Khan, W. A. & Sajid, M. Consequence of convective conditions for the flow of Oldroyd-B nanofluid by a stretching cylinder. *J. Braz. Soc. Mech. Sci. Eng.* **41**, 116 (2019).
37. Tlili, I., Waqas, H., Almaneea, A., Khan, S. U. & Imran, M. Activation energy, and second-order slip in bioconvection of oldroyd-B nanofluid over a stretching cylinder: A proposed mathematical model. *Processes* **7**, 914 (2019).
38. Waqas, H., Shehzad, S. A., Khan, S. U. & Imran, M. Novel numerical computations on flow of nanoparticles in porous rotating disk with multiple slip effects and microorganisms. *J. Nanofluids* **8**, 1423–1432 (2019).
39. Shafiq, A., Rasool, G., Khalique, C. M. & Aslam, S. Second grade bioconvective nanofluid flow with buoyancy effect and chemical reaction. *Symmetry.* **12**, 621 (2020).
40. Khan, S. U., Waqas, H., Bhatti, M. M. & Imran, M. Bioconvection in the rheology of magnetized couple stress nanofluid featuring activation energy and Wu's slip. *J. Non-Equilib. Thermodyn.* **45**, 81–95 (2020).
41. Wang, Y., Waqas, H., Tahir, M., Imran, M. & Jung, C. Y. Effective Prandtl aspects on bio-convective thermally developed magnetized tangent hyperbolic nanoliquid with gyrotactic microorganisms and second-order velocity slip. *IEEE Access* **7**, 130008–130023 (2019).
42. Shafiq, A., Hammouch, Z. & Sindhu, T. N. Bioconvective MHD flow of tangent hyperbolic nanofluid with Newtonian heating. *Int. J. Mech. Sci.* **133**, 759–766 (2017).
43. Khan, S. U., Rauf, A., Shehzad, S. A., Abbas, Z. & Javed, T. Study of bioconvection flow in Oldroyd-B nanofluid with motile organisms and effective Prandtl approach. *Physica A Stat. Mech. Appl.* **527**, 121179 (2019).
44. Li, Y. *et al.* A numerical exploration of modified second-grade nanofluid with motile microorganisms, thermal radiation, and Wu's slip. *Symmetry* **12**(3), 393 (2020).
45. Farooq, U. *et al.* Thermally radioactive bioconvection flow of Carreau nanofluid with modified Cattaneo–Christov expressions and exponential space-based heat source. *Alex. Eng. J.* **60**, 3073–3086 (2021).
46. Song, Y. Q. *et al.* Bioconvection analysis for Sutterby nanofluid over an axially stretched cylinder with melting heat transfer and variable thermal features: A Marangoni and solutal model. *Alex. Eng. J.* **60**, 4663–4675 (2021).
47. Al-Mubaddel, F. S. *et al.* Double stratified analysis for bioconvection radiative flow of Sisko nanofluid with generalized heat/mass fluxes. *Phys. Scr.* **96**, 055004 (2021).
48. Shaheen, N., Ramzan, M., Alshehri, A., Shah, Z. & Kumam, P. Sort-Dufour impact on a three-dimensional Casson nanofluid flow with dust particles and variable characteristics in a permeable media. *Sci. Rep.* **11**, 1–21 (2021).
49. Chu, Y. M. *et al.* Numerical simulation of squeezing flow Jeffrey nanofluid confined by two parallel disks with the help of chemical reaction: Effects of activation energy and microorganisms. *Int. J. Chem. React. Eng.* **19**, 717–725 (2021).
50. Khan, M. I. *et al.* Assessment of bioconvection in magnetized Sutterby nanofluid configured by a rotating disk: A numerical approach. *Mod. Phys. Lett. B* **35**, 2150202 (2021).
51. Waqas, H., Farooq, U., Ibrahim, A., Shah, Z. & Kumam, P. Numerical simulation for bioconvectional flow of burger nanofluid with effects of activation energy and exponential heat source/sink over an inclined wall under the swimming microorganisms. *Sci. Rep.* **11**, 1–15 (2021).
52. Babazadeh, H., Shah, Z., Ullah, I., Kumam, P. & Shafee, A. Analysis of hybrid nanofluid behavior within a porous cavity including Lorentz forces and radiation impacts. *J. Therm. Anal. Calorim.* **143**, 1129–1137 (2020).
53. Waqas, H., Farooq, U., Muhammad, T., Hussain, S. & Khan, I. Thermal effect on bioconvection flow of Sutterby nanofluid between two rotating disks with motile microorganisms. *Case Stud. Thermal Eng.* **26**, 101136 (2021).
54. Imran, M., Farooq, U., Muhammad, T., Khan, S. U. & Waqas, H. Bioconvection transport of Carreau nanofluid with magnetic dipole and nonlinear thermal radiation. *Case Stud. Thermal Eng.* **26**, 101129 (2021).
55. Waqas, H., Farooq, U., Shah, Z., Kumam, P. & Shutaywi, M. Second-order slip effect on bio-convectional viscoelastic nanofluid flow through a stretching cylinder with swimming microorganisms and melting phenomenon. *Sci. Rep.* **11**, 1–16 (2021).
56. Jawad, M. *et al.* Entropy generation and heat transfer analysis in MHD unsteady rotating flow for aqueous suspensions of carbon nanotubes with nonlinear thermal radiation and viscous dissipation effect. *Entropy* **21**, 492 (2019).
57. Hayat, T., Muhammad, T., Shehzad, S. A. & Alsaedi, A. Three-dimensional boundary layer flow of Maxwell nanofluid: a mathematical model. *Appl. Math. Mech.* **36**(6), 747–762 (2015).
58. Wakif, A. & Sehaqui, R. Generalized differential quadrature scrutinization of an advanced MHD stability problem concerned water-based nanofluids with metal/metal oxide nanomaterials: A proper application of the revised two-phase nanofluid model with convective heating and through-flow boundary conditions. *Numer. Methods Partial Differ. Equ.* (2020).
59. Wakif, A., Animasaun, I. L., Narayana, P. S. & Sarojamma, G. Meta-analysis on thermo-migration of tiny/nano-sized particles in the motion of various fluids. *Chin. J. Phys.* **68**, 293–307 (2019).
60. Chhabra, R. P. & Richardson, J. F. *Non-Newtonian Flow and Applied Rheology: Engineering Applications* (Butterworth-Heinemann, 2011).

Acknowledgements

"The authors acknowledge the financial support provided by the Center of Excellence in Theoretical and Computational Science (TaCS-CoE), KMUTT". Moreover, this research project is supported by Thailand Science Research and Innovation (TSRI) Basic Research Fund: Fiscal year 2021 under Project Number 64A306000005.

Author contributions

U.F. and Z.S. modeled and solved the problem. H.W. and U.F. wrote the manuscript. P.K. and W.D. acontributed in the numerical computations and plotting the graphical results. All authors finalized the manuscript after its internal evaluation.

Competing interests
The authors declare no competing interests.

Additional information
Correspondence and requests for materials should be addressed to Z.S. or P.K.

Reprints and permissions information is available at www.nature.com/reprints.

Publisher's note Springer Nature remains neutral with regard to jurisdictional claims in published maps and institutional affiliations.

Open Access This article is licensed under a Creative Commons Attribution 4.0 International License, which permits use, sharing, adaptation, distribution and reproduction in any medium or format, as long as you give appropriate credit to the original author(s) and the source, provide a link to the Creative Commons licence, and indicate if changes were made. The images or other third party material in this article are included in the article's Creative Commons licence, unless indicated otherwise in a credit line to the material. If material is not included in the article's Creative Commons licence and your intended use is not permitted by statutory regulation or exceeds the permitted use, you will need to obtain permission directly from the copyright holder. To view a copy of this licence, visit http://creativecommons.org/licenses/by/4.0/.

© The Author(s) 2022